How Does Thermal Poling Affect the Structure of Soda-Lime Glass?

ARTICLE · JUNE 2010

CITATIONS
7

READS
65

2 AUTHORS, INCLUDING:

Vincent Rodriguez
University of Bordeaux
172 PUBLICATIONS **1,926** CITATIONS

SEE PROFILE

How Does Thermal Poling Affect the Structure of Soda-Lime Glass?

Marc Dussauze* and Vincent Rodriguez

Institut des Sciences Moléculaires, UMR 5255 CNRS, Université de Bordeaux, 351 cours de la Libération, 33405 Talence Cedex, France

Andrey Lipovskii and Michael Petrov

St. Petersburg State Polytechnical University, Polytechnicheskaja 29, St. Petersburg, 195251, Russia

Charmayne Smith and Kathleen Richardson

School of Materials Science and Engineering, Clemson University, COMSET, 161 Sirrine Hall, Box 340971, Clemson, South Carolina 29634, USA

Thierry Cardinal and Eveline Fargin

Institut de Chimie de la Matière Condensée de Bordeaux - UPR 9048 CNRS université de Bordeaux, Avenue du Dr. Schweitzer, 33608 Pessac Cedex, France

E. I. Kamitsos

Theoretical and Physical Chemistry Institute, National Hellenic Research Foundation, 48 Vass. Constantinou Ave., 116 35 Athens, Greece

Received: April 15, 2010; Revised Manuscript Received: June 10, 2010

Soda lime glasses polarized either with an open or a blocking anode have been characterized by IR reflectance spectroscopy and a combined analysis of second harmonic generation and Raman imaging. The experimental results clearly show that the electrode nature influences strongly (i) the thickness of the space charge layer, (ii) the $\chi^{(2)}$ efficiency, and (iii) the structural rearrangements. Besides, using theoretical models accounting for charge carriers' mobilities, the respective influence of two distinct compensation mechanisms, that is an injection of positive charges (H_3O^+/H^+ ions) or a drift of oxygen ions, have been confirmed.

1. Introduction

Presently, thermal poling of vitreous silica and soft silica-based glasses is in use to provide second harmonic generation[1] and Pockels electro-optical sensitivity[2,3] to these initially isotropic materials. The breaking of central symmetry of glasses under an electric field has been attributed to negative charges[4] formed in the course of glass poling and "frozen" when it is cooled under the applied voltage. Negative charges are formed due to the depletion of the subanodic glass region from positive charge carriers, that is alkali and alkali-earth ions, which move under a very high electric field with magnitudes of up to volts per nanometers in a several micrometer-size thick layer beneath the anode.[5] It has been argued elsewhere[6] that these negative charges are associated with nonbridging oxygen atoms, which are partially compensated, otherwise the thickness of the charged layer could hardly exceed tens of nanometers in accordance with the single charge motion model developed by Von Hippel.[7] In the case of poling with open anode, that is with electrode allowing contact of the anodic surface of glass under poling with the atmosphere, the essential compensation of the negatively charged nonbridging oxygen atoms is proposed to be due to the injection of positively charged species of atmosphere origin into the glass of most probably H_3O^+/H^+ ions.[4,8] This process results in bonding of hydrogen with nonbridging oxygen in glass and, thus, in neutralization of the negative charge. The presence of oxygen-bonded hydrogen in poled glasses has been observed frequently.[4,9] In the case of the anodic electrode preventing the contact of glass with the atmosphere, like metal films deposited by vacuum sputtering[4,10] (poling with so-called blocking anode), poling in vacuum[11] or in inert atmosphere,[12] the depth of the alkali-depleted region also falls in the micrometer range and the negative charge is also compensated. The mechanism of this compensation is not clear yet, and the majority of studies performed with poled glasses provide no explanation for it. Generally, in soft silicate glasses, like the widely used soda-lime glass in poling experiments, there are only two species that are negatively charged; oxygen ions and electrons.

The possibility of the drift of oxygen ions, as discussed originally by Carlson,[10] is accepted by the "anodic bonding community", contrary to the "glass poling community". Nevertheless, anodic bonding and glass poling deal with the same process, and ideas related to the possibility of oxygen ion motion were presented recently in discussions of glass poling processes.[5,6,13] Direct measurements indicating some oxygen depletion in the subsurface layer of glass after anodic bonding have been reported recently,[14,15] and studies of charge equilibrium in poled glasses performed simultaneously with infrared spectroscopy also proposed an oxygen deficit in the poled region of glasses.[16] The possibility of electronic conductivity in glasses is usually rejected, except for the poling of glass−metal nanocomposites.[17]

* To whom correspondence should be addressed. E-mail: m.dussauze@ism.u-bordeaux1.fr.

10.1021/jp1033905
Published on Web 07/01/2010

Nevertheless, charge compensation via motion of electrons in the course of glass poling was considered by Krieger[18] in a detailed study of this process. It was concluded that electrons in the studied glass are capable of moving under the very high electric field in the subanodic region by hopping through nonbridging oxygen sites while oxygen itself does not move.

If movement of oxygen ions or removal of electrons from nonbridging oxygen atoms involves a restructuring of the silicate glass network, vibrational spectroscopy should be capable of providing relevant information. In this work, we present results of infrared, μ-Raman, and μ-second harmonic generation (μ-SHG) studies of soda-lime glasses poled either with blocking or open anodes. The observed evolution of the size of the poled region is compared with that given by models developed for the cases of positive charges (H_3O^+/H^+ ions) and negative charges (oxygen ions) moving in the course of glass poling.

2. Experimental Details

The glass explored was a commercially available soda lime glass (SLG) with composition 72.20% SiO_2, 14.30% Na_2O, 6.40% CaO, 4.30% MgO, 1.20% K_2O, and 1.20% Al_2O_3 (weight %). The thickness of each glass plates was 1 mm.

Poling treatments were done either in air (open electrode) or in argon (blocking electrode) atmosphere at normal pressure. The soda lime glasses were heated to a poling temperature of 210 °C and polarized with a 1.5 kV voltage applied for 40 min after the poling temperature was reached. For both poling conditions (i.e., either air-poled or Ar-poled), unpolished silicon wafers were used at the anode to create a thin and reproducible gap between the anode electrode and the glass surface.

The IR spectra were recorded on a Nexus 670 spectrophotometer (Thermo Optek) equipped with a DTGS detector and a germanium-coated KBr beam splitter or hybrid FIR beam splitter. A total of 200 scans were averaged with a resolution of 4 cm^{-1}. The spectrometer was purged with dry air to minimize atmospheric CO_2 and water vapor. Reflectance experiments were performed using an external reflection attachment (Graesby, Specac) at an angle of incidence of 12°. Absorbance spectra were calculated from the reflectance spectra by the Kramers−Kronig analysis.

We used in this study a combined analysis of (i) μ-Raman scattering spectroscopy and (ii) μ-SHG in the reflection mode, using the same setup to gain a direct link between physical properties and local structure. The experimental setup is based on a modified μ-Raman HR800 (Horiba/Jobin-Yvon) instrument equipped with two laser sources (picosecond laser at 1064 nm -hyper-Raman and SHG, CW laser at 532 nm - Raman). Confocal microscopy and motorized stages (X, Y, Z) allows 3D investigation. The μ-Raman spectra were recorded with a typical resolution of 2.5 cm^{-1} in the backscattering geometry at room temperature. More details about the μ-spectrometer setup and its ability are given elsewhere.[19]

3. Infrared and Combined Raman/SHG Microscopies

Part A of Figure 1 shows the transmission spectra in the mid-infrared spectral region of soda-lime glasses before and after poling in air atmosphere. Both spectra exhibit absorptions at ca. 3530 and 2880 cm^{-1} attributed to O−H stretching of silanol groups (SiOH) in the silicate network.[20] In particular, the higher frequency component can be assigned to "free OH", whereas the shoulder at ca. 2880 cm^{-1} signifies the presence of hydrogen-bonded OH groups. Part A of Figure 1 demonstrates a considerable increase of the intensity of the 3530 cm^{-1} band after the poling treatment in air, whereas no changes were

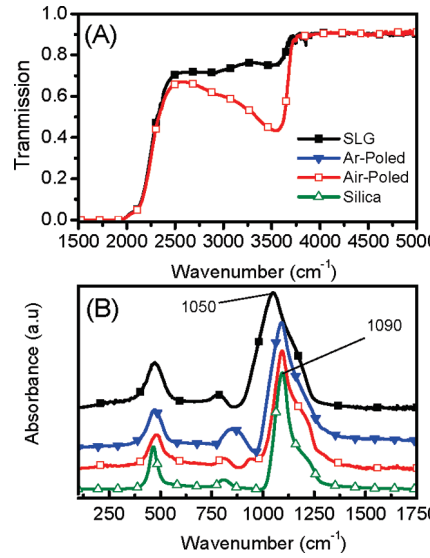

Figure 1. (A) IR transmittance spectra of initial and air-poled soda-lime glass (SLG) samples. (B) Absorbance spectra obtained from the KK-transformed reflectance spectra measured at the anode side of air-poled and Ar-poled soda-lime glasses. For comparison, spectra of silica (infrasil) and (initial) soda-lime glasses are included.

observed in the corresponding spectrum of the sample poled in Ar-atmosphere (not reported).

Below 2000 cm^{-1}, the transmission of the studied glasses is practically zero and, thus IR reflectance spectroscopy becomes convenient for probing structural changes at interfaces, with typical micrometric depth sensitivity depending on the energy range. Part B of Figure 1 compares the Kramers−Kronig transformed reflectance spectra (presented in the absorbance form) of argon- and air-poled samples with the spectra of two as-prepared silicate glasses; soda lime glass and pure silica (infrasil type).

Three broad bands are observed in the spectra of part B of Figure 1; 400−550 cm^{-1}, 700−850 cm^{-1}, 950−1250 cm^{-1}. The low-frequency band (400−550 cm^{-1}) is attributed to the rocking motion of Si−O−Si bridges, whereas the corresponding bending mode is responsible for absorption at 700−850 cm^{-1}. The intense band ranging from 950 to 1250 cm^{-1} originates from asymmetric stretching vibrations of Si−O−Si bridges and $Si-O^-$ nonbridging bonds in Q^n tetrahedral entities (where n is the number of bridging oxygen atoms per silicon tetrahedron). By reference to previous works on pure silica and modified silicate glasses, we expect for a fully connected silicate network (i.e., only Q^4 entities), the main absorption at 1090 cm^{-1} and a shoulder at ca. 1200 cm^{-1} both related to Si−O−Si asymmetric vibrations, and a gradual shift to lower frequency of the main absorption band to ca. 1075 cm^{-1} and 935 cm^{-1} for Q^3 and Q^2 sites, respectively.[21−23]

After thermal poling treatments either in air or in argon, similar effects are observed on the high frequency band, which becomes narrower and shifts from 1050 cm^{-1} (soda-lime) toward 1090 cm^{-1} (silica). These spectral changes clearly denote that for both poled soda-lime samples the structure, which was initially composed of a majority of Q^3 units, has transformed toward a glassy network where Q^4 entities are predominant. Thus, thermal poling appears to lead to a silica-like network in terms of the high-frequency infrared profile. However, the lower frequency range of the poled glasses where the rocking and bending modes of Si−O−Si bridges are active has not reached yet the characteristics of silica. This may be due to the fact that these modes are more sensitive to neighboring structural units,

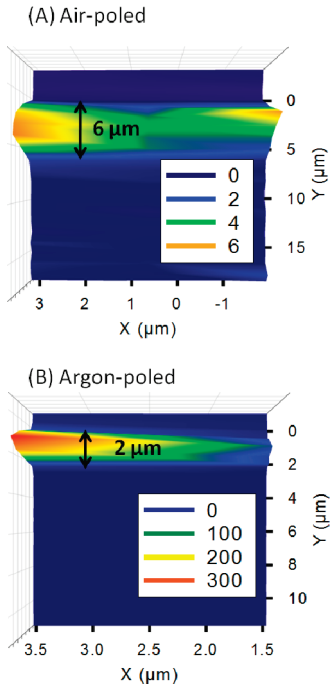

Figure 2. SHG images measured on the cross section of (A) air-poled and (B) argon-poled soda-lime glasses. *(SHG magnitude is in arbitrary units; the position Y = 0 corresponds to the anode surface and positive values of Y are toward the cathode side).*

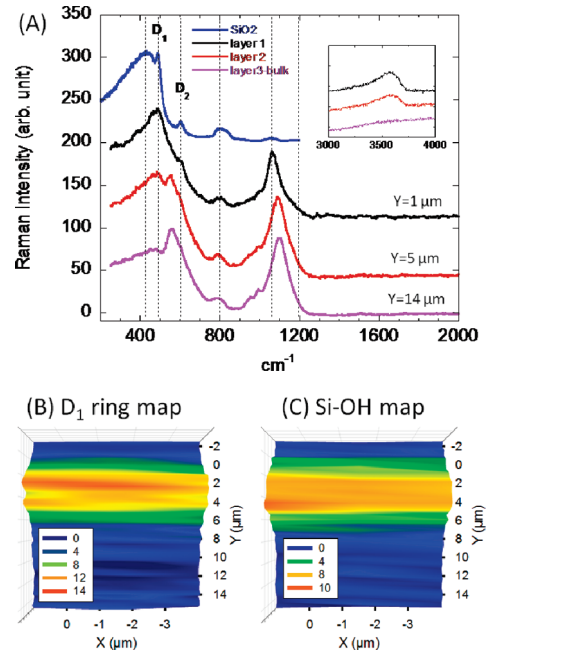

Figure 3. (A) Raman spectra of a SiO_2 glass (reference) and three representative spectra collected on the cross section of the air-poled soda-lime sample. (B) Raman mapping of the "D_1 mode" (C) Raman mapping linked to the hydroxyl group vibration. *(The position Y = 0 corresponds to the anode surface and positive value of Y are toward the cathode side).*

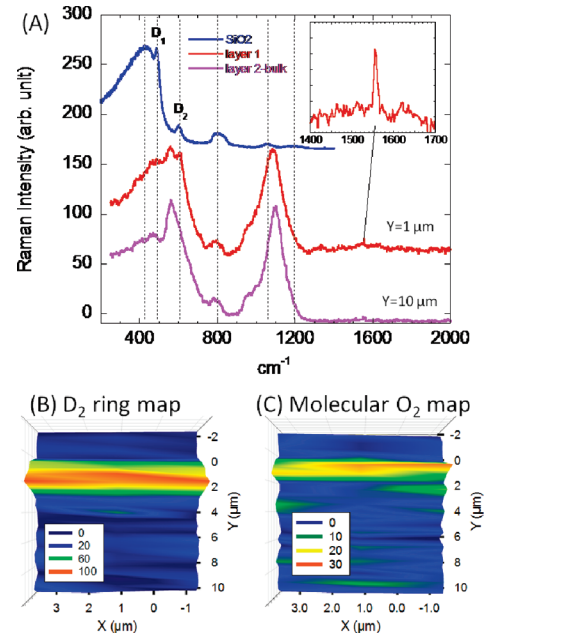

Figure 4. (A) Raman spectra of a SiO_2 glass (reference) and two representative spectra collected on the cross section of the argon-poled soda lime sample. (B) Raman mapping of the "D_2 mode" (C) Raman mapping linked to the O_2 vibration. *(The position Y = 0 corresponds to the anode surface and positive value of Y are toward the cathode side).*

indicating that the 3D interconnection of the network of poled glasses has not achieved yet the degree exhibited by silica glass.

To get additional insights into thermal poling effects, we have combined second harmonic and Raman imaging of the cross section of air- and argon-poled soda-lime glasses. Our procedure was to first localize and then map the NLO layer using second harmonic generation microscopy and, in a second step, to record the corresponding μ-Raman map at the same sample area. Such a protocol warrant direct correlations between NLO properties and vibrational/structural features. The SHG images of air- and argon-poled glasses are reported in parts A and B of Figure 2. They clearly show the influence of the atmosphere during poling both on the SHG efficiency and on the thickness of the NLO layer. Even though the two samples have been thermally polarized under the same conditions of voltage and temperature, the air-poled sample has a NLO layer 6 μm thick, whereas it is 2 μm thick in the case of the argon-poled glass. In parallel, it is noted that there is a large difference in SHG signal intensity, which is 50 times lower in the air-poled NLO layer.

Figures 3 and 4 give Raman spectra and images of the air- and argon-poled samples, respectively. Both figures include the Raman spectrum of pure silica for comparison purposes. Part A of Figure shows three spectra recorded along the cross section of the air-poled glass; two within the space charge layer (1and 5 μm below the anode interface) and one in the region where no SHG signal has been detected (14 μm below the anode interface). Similarly, two spectra from the argon-poled sample have been selected and are shown in part A of Figure 4; one measured within the SHG active layer (1 μm) and the other one recorded 10 μm below the anode surface. Note first that for both poled samples the Raman spectra collected in SHG-inactive areas (e.g., Figure 3: $Y = 14$ μm; Figure 4: $Y = 10$ μm) are identical to the spectrum of the initial soda-lime glass (not reported). They exhibit two main contributions, the one at 1100 cm^{-1} attributed to the symmetric stretching of Q^3 units, which involves mainly the $Si-O^-$ nonbridging bonds and the other at 540 cm^{-1} with a broad shoulder around 450 cm^{-1} due to mixed stretching-bending vibrational modes of Si−O−Si bridges.[21,24]

Interestingly, several spectral variations are observed within the space charge layer. In the case of the air-poled sample (Figure 3), we observe a decrease of the relative intensity of the bands at 1100 cm^{-1} and 540 cm^{-1} and an increase of intensity in the spectral region of Si−O−Si stretching-bending

with a maximum at 485 cm^{-1} and a weak shoulder at 605 cm^{-1}. According to Raman studies of silica, we attribute the new contributions at 485 cm^{-1} and 605 cm^{-1} to the symmetric stretching vibration of Si−O−Si bridges in four-member and three-member rings of SiO_4 tetrahedra, respectively, the larger rings commonly called D_1 defect and the smaller ones D_2 defect.[25] In addition, we note the growth of a new broad band due to hydroxyl groups (OH) around 3600 cm^{-1} (insert in part A of Figure 3).

Parts B and C of Figure 3 report the Raman mapping of the 485 cm^{-1} (D_1 ring) and the 3600 cm^{-1} (hydroxyl group) bands. The comparison between these two Raman images and the SHG image (part A of Figure 2) denotes a good spatial correspondence between NLO activity and structural changes down to 6 μm. Moreover, the observed Raman modifications are in agreement with the conclusions from IR transmittance and reflectance studies. It is also remarked that the parallel behavior exhibited by D_1 defects and hydroxyl groups in the air-poled sample is in accordance with their variation observed in sol−gel silica heat-treated up to 1000 °C.[22] In this context, we suggest that poling under air triggers an increase of the population of Q^4 units with resulting Si−O−Si bridges building up ring structures (D_1 types) but at a less extent than in sol−gel silica.

The variations observed in the Raman spectra of the argon-poled sample differ from those of the air-poled sample. While poling causes again an intensity decrease of the band at 540 cm^{-1}, the D_2 band at 605 cm^{-1} gains intensity and signifies an increase of the population of Si−O−Si bridges in three-member rings. Part B of Figure 3 reports the mapping of this D_2 band and points out a good spatial correspondence with the SHG active layer (part B of Figure 2). In addition to these findings, we note the appearance of a weak but very sharp band at 1550 cm^{-1} in the insert in part A of Figure 4. As evidenced in the image shown in part C of Figure 4, the band at 1550 cm^{-1} is observed exclusively in the space charge layer. In accordance with previous studies in gases dissolved in glass or the effects of β-irradiation on silicate glasses, we assign the very sharp feature at 1550 cm^{-1} to molecular oxygen dissolved in the glass matrix.[26−28]

4. Discussion and Modeling of H_3O^+/H^+ Ions and Oxygen Motion in Glass

The nature of the anode electrode is expected to influence the kind of compensation mechanism occurring during poling as triggered by the depletion in mobile cations, such as Na^+ or Ca^{2+} ions in soda-lime glass.[29] Concerning the present experimental results, the formation of hydroxyl group detected by IR and Raman spectroscopy only in case of the air-poled glass would tend to suggest that it is possible to differentiate substantially between the two electrode configurations. However, for both atmospheric conditions employed here we have observed a common characteristic namely the increase in the degree of polymerization of the silicate network within the space charge zone. As already discussed for other glass systems,[6] such an increase in the population of bridging bonds within the silicate network would result from a loss of nonbridging oxygen atoms, denoting an important participation of anionic conduction by oxygen ions during poling. Thus, it turns out that (i) for the air-poled sample both H_3O^+/H^+ ions injection and, partly, nonbridging oxygen removal take place as compensation mechanisms, and (ii) for the argon-poled sample no H_3O^+/H^+ ions injection was detected, but structural rearrangements inducing anionic conduction through release of nonbridging oxygen atoms appear to be the predominant compensation mechanism.

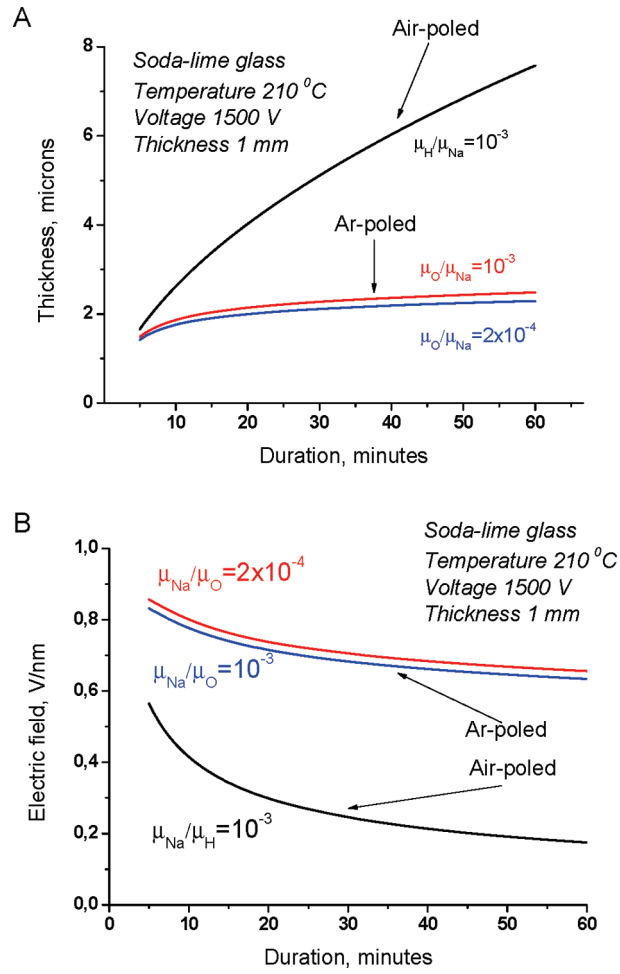

Figure 5. A: Modeling of temporal dependence of the thickness of subanodic depleted layer for poling soda-lime glass with open (air-poled glass) and blocking (Ar-poled glass) anodes. B: Modeling of temporal dependence of the maximum magnitude of the electric field in subanodic depleted layer for poling soda-lime glass with open (air-poled glass) and blocking (Ar-poled glass) anodes.

With these facts in mind, we aim now to compare the present experimental results with predictions of theoretical models proposed in the literature. By assuming almost complete replacement of Na^+ by H_3O^+/H^+ ions, and neglecting the drift of other positive ions like calcium, we use the formalism developed by Prieto and Linares[30] to calculate the dependence of sodium-depleted thickness with time and applied voltage, as well as the electric field distribution in glass. For the poling conditions of this work, that is 1 mm thick soda-lime glass under applied voltage of 1.5 kV at ~210C, and for a ratio of ionic mobilities $\mu_{Na}/\mu_H = 1000$,[31] the calculated time dependence of the thickness of the depleted layer is shown in part A of Figure 5. Here, we used the relation[30] to calculate the thickness d_H of hydrogen-enriched layer:

$$d_H = \frac{\gamma}{1-\gamma}\left(\sqrt{\frac{2(1-\gamma)}{\gamma^2}\mu_H U t + L^2} - L\right)$$

where $\gamma = (\mu_H)/(\mu_{Na})$, the relation of sodium and H_3O^+/H^+ ions mobilities, L is the thickness of glass, and U is the voltage applied. To evaluate electric field in sodium-depleted region we used the relation $E_H(t) = (U)/(d_H(t) + \gamma(L - d_H(t)))$, which can be easily deduced from the consideration developed in ref 30. The only parameter influencing the thickness of depleted

layer in used model is the relation of H_3O^+/H^+ ions and sodium ionic motilities. Within the frames of this model, where we neglect thermal diffusion, there is no depth dependence of the field magnitude within the hydrogen-enriched layer.

The result shows that the thickness of the layer is growing monotonically. According to the model, an increase of the applied voltage works the same way as time does. In parallel with the increase of the thickness of the depleted layer, the amplitude of the electric field drops in the layer (curve for air-poled glass, part B of Figure 5). Assuming a "freezing" of this field after poling, one would expect a decrease of glass nonlinearity for longer poling time in the case that only positive charges participate in the poling process.

The model accounting for the motion of negative charge carriers (oxygen ions) in the course of glass poling supposes exponential growth of their mobility with the magnitude of electric field due to the field-induced decrease of negative ion activation energy:[10]

$$\mu_o = \mu_o^0 \exp\left(\frac{E}{E_0}\right), E_0 = \frac{2\varepsilon kT}{ea}$$

where E is electrical field, ε is dielectric permittivity of the glass, a is mean jump length of oxygen ions, that is the mean distance between nonbriging oxygen sites in the virgin glass, kT is thermal energy, and μ_o^0 is oxygen ions mobility in weak fields. The expression for oxygen mobility allows us to write the system of differential equations where we neglect thermal diffusion of participating ions:

$$\frac{\partial C_{Na}}{\partial t} + \frac{\partial}{\partial x}\mu_{Na} C_{Na} E = 0$$
$$\frac{\partial C_O}{\partial t} - \frac{\partial}{\partial x}\mu_O(E) C_O E = 0$$
$$\frac{\partial E}{\partial x} = \frac{e}{\varepsilon\varepsilon_0}(C_{Na} - C_O)$$

with initial conditions:

$$C_{Na}\Big|_{t=0} = C_O\Big|_{t=0} = C_{Na}^0$$
$$E\Big|_{t=0} = \frac{U}{L}$$

and additional condition for the field

$$\int_0^L E(x,t)\mathrm{d}x = U$$

Here, C_{Na},C_O are sodium and nonbridging oxygen concentrations, C_{Na}^0 is sodium concentration in the virgin glass, μ_{Na} is sodium mobility in the glass, and $\mu_O(E)$ is field-dependent oxygen mobility. The developed model neglects the penetration of atmospheric hydrogenated species in the glass, that is it corresponds to the case of a blocking anode. A numerical solution of the equations for soda-lime glass (evaluated using the composition of the glass, a = ~0.7 nm.) under the same poling conditions and using the same parameters as for the calculation with H_3O^+/H^+ ions, allowed us to calculate the temporal dependence of the modified layer thickness. In this

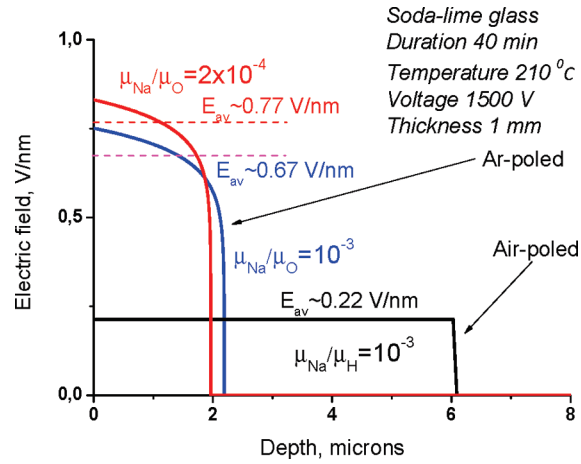

Figure 6. Modeling of electric field distribution in the subanodic depleted layer for poling soda-lime glass with open (air-poled glass) and blocking (Ar-poled glass) anodes. Average magnitudes of electric field are marked near corresponding graphs.

case, we had no preliminary information about the mobility of oxygen ions, and, thus, several values of the mobility were used. Performed modeling showed that the corresponding dependences do not change essentially even with oxygen ion mobility varying by more than an order of magnitude. The modeled thickness (curves for Ar-poled glass, part A of Figure 5) and the maximum magnitude of the electric field in the depleted layer (curves for Ar-poled glass, part B of Figure 5) are presented for ratios of sodium and oxygen ionic mobilities in glass $\mu_O/\mu_{Na} = 10^{-3}$, and $\mu_O/\mu_{Na} = 2 \times 10^{-4}$. It is noted that the depleted layer saturates in the case of oxygen motion, that is the depth of depletion stays limited. A thinner layer results in a higher electric field, as shown by curves for Ar-poled glass in part B of Figure 5. According to the model developed, one expects a higher frozen electric field and, as a consequence, a higher optical nonlinearity in glasses poled with blocking anode. This nonlinearity is localized in a layer the thickness of which stops to increase at longer poling time.

We have calculated the distribution of electric field in poled layers for soda-lime glass poled in air and argon for 40 min. The results in Figure 6 show that the values of the thickness and electric field of the space charge layer are in reasonable agreement with our experimental measurements.

The argon-poled sample, for which no charge injection has been detected, has a space charge depth of 2 μm as predicted by the model. We obtain in the case of the air poled sample a depth of 6 μm that corresponds well to experiment. Moreover, the amplitude of the embedded electric field can be extrapolated through the SHG response since in the case of a pure EFISH process (electric field induce second harmonic) the $\chi^{(2)}$ response is expressed as: $\chi^{(2)} = 3 \cdot \chi^{(3)} \cdot E_{int}$. Assuming no $\chi^{(3)}$ modification in the space charge layer, we can compare/scale the experimental $\chi^{(2)}$ ratio with the predicted electric fields ratio, $E_{open}/E_{blocking}$ = ~0.3. From our micro-SHG data one can expect $\chi^{(2)}{}_{\text{air-poled}}/\chi^{(2)}{}_{\text{argon-poled}} \sim (I_{\text{SHG air-poled}}/I_{\text{SHG argon-poled}})^{0.5}$ which gives a ratio of 0.14. Here again, the correspondence between experimental and calculated results is considered acceptable.

Finally, two important remarks can be drawn. The first concerns the evidence for molecular oxygen, O_2, dissolved in the glass matrix within the space charge layer in the case of a fully blocking electrode (argon-poled sample). This finding denotes the importance of $Si-O^-$ bond breaking as a charge compensation mechanism. In addition, this points out a complex anionic conduction of oxygen ions within the glass network and

the formation of neutral isolated species trapped in the glass matrix. Second, we have demonstrated that two coexisting mechanisms having different effective thicknesses because of different mobilities of the involved mobile ions occur for poling under air. Such a poling might induce the formation of "layered" subanodic structures, especially when higher voltages are applied.

5. Conclusions

This work has clearly demonstrated that a strong electric field formed during poling of glasses initiates complex motions of different charge carriers, and this influences differently SHG response and structural rearrangements. Under a blocking anode configuration (argon-poled sample), the main compensation mechanism is linked to the release of nonbridging oxygen as evidenced by molecular oxygen trapped within the glass matrix. Poling treatment under air induces an intermediate open/blocking electrode regime. The structural rearrangements triggered by the migration of nonbridging oxygen lead to the formation of four-member (D_1) and three-member (D_2) silicate rings in relative populations depending on the electrode nature. Finally, both calculations and experimental data have shown clearly the large influence of type of electrode on the space charge layer thickness and the implemented electric field.

Acknowledgment. M.D. and V.R. thank Frédéric Adamietz, David Talaga, and Jean-Luc Bruneel for technical assistance. This research has been supported by Région Aquitaine (Advanced Materials in Aquitaine - Lasinof), the Agence Nationale de la Recherche ANR (grant ANR-05-BLAN-0212-01), and by the EU through the Marie Curie Actions-NANONLO project (MTKD-CT-2006-042301). M.P. thanks Russian Ministry for Education and Science (grant No 2.1.1/988). A.L. thanks the Russian Foundation for Basic Research (grant 08-02-00522).

References and Notes

(1) Myers, R. A.; Mukherhee, N.; Brueck, S. R. J. *Opt. Lett.* **1991**, *16*, 1732.
(2) Ren, Y.; Marckmann, C. J.; Arentoft, J.; Kristensen, M. *IEEE Photonics Technology Letters* **2002**, *14*, 639.
(3) Long, X. C.; Brueck, S. R. J. *IEEE Photonics Technology Letters* **1997**, *9*, 767.
(4) Lepienski, C. M.; Giacometti, J. A.; Ferreira, G. F. L.; Freire, F. L.; Achete, C. A. *J. Non-Cryst. Solids* **1993**, *159*, 204.
(5) Fabbri, M.; Senna, J. R. *J. Electrochem. Soc.* **2008**, *155*, G274.
(6) Dussauze, M.; Kamitsos, E. I.; Fargin, E.; Rodriguez, V. *J. Phys. Chem. C* **2007**, *111*, 14560.
(7) von Hippel, A.; Gross, E. P.; Jelatis, J. G.; Geller, M. *Phys. Rev.* **1953**, *91*, 568.
(8) Doremus, R. H. *J. Non-Cryst. Solids* **1975**, *19*, 137–44.
(9) Deparis, O.; Kazansky, P. G.; Podlipensky, A.; Abdolvand, A.; Seifert, G.; Graener, H. *Appl. Phys. Lett.* **2005**, *86*, 261109.
(10) Carlson, D. E.; Hang, K. W.; Stockdal, G. F. *J. Am. Ceram. Soc.* **1974**, *57*, 295. Carlson, D. E.; Hang, K. W.; Stockdale, G. F. *J. Am. Ceram. Soc.* **1972**, *55*, 337. Carlson, D. E. *J. Am. Ceram. Soc.* **1974**, *57*, 291.
(11) Pruneri, V.; Samoggia, F.; Bonfrate, G.; Kazansky, P. G.; Yang, G. M. *Appl. Phys. Lett.* **1999**, *74*, 2423.
(12) Moncke, D.; Dussauze, M.; Kamitsos, E. I.; Varsamis, C. P. E. *Phys. Chem. Glasses: Eur. J. Glass Sci. Technol. B* **2009**, *50*, 229.
(13) Ziemath, E. C.; Arauljo, V. D.; Escanhoela, J. *J. Appl. Phys.* **2008**, *104*, 054912.
(14) Nitzsche, P.; Lange, K.; Schmidt, B.; Grigull, S.; Kreissig, U.; Thomas, B.; Herzog, K. *J. Electrochem. Soc.* **1998**, *145*, 1755.
(15) Schmidt, B.; Nitzsche, P.; Lange, K.; Grigull, S.; Kreissig, U.; Thomas, B.; Herzog, K. *Sensors Actuators A* **1998**, *67*, 191.
(16) Dussauze, M.; Rodriguez, V.; Velli, L.; Varsamis, C. P. E.; Kamitsos, E. I. *J. Appl. Phys.* **2010**, *107*, 043505.
(17) Deparis, O.; Kazansky, P. G.; Podlipensky, A.; Abdolvand, A.; Seifert, G.; Graener, H. *J. Appl. Phys.* **2006**, *100*, 044318.
(18) Krieger, U. V.; Lanford, W. A. *J. Non-Cryst. Solids* **1988**, *102*, 50.
(19) Rodriguez, V.; Talaga, D.; Adamietz, F.; Bruneel, J. L.; Couzi, M. *Chem. Phys. Lett.* **2006**, *431*, 190.
(20) Nieto, M. I.; Duran, A.; Navarro, J. M. F.; Mazo, J. L. O. *J. Am. Ceram. Soc.* **1984**, *67*, 242.
(21) Merzbacher, C. I.; White, W. B. *J. Non-Cryst. Solids* **1991**, *130*, 18.
(22) Kamitsos, E. I.; Patsis, A. P.; Kordas, G. *Phys. Rev. B* **1993**, *48*, 12499. Kamitsos, E. I. *Phys. Rev. B* **1996**, *53*, 14659.
(23) Kapoutsis, J. A.; Kamitsos, E. I.; Chryssikos, G. D.; Yiannopoulos, Y. D.; Patsis, A. P.; Prassas, M. *Chimica Chronica* **1994**, *23*, 341–346. Ingram, M. D.; Davidson, J. E.; Coats, A. M.; Kamitsos, E. I.; Kapoutsis, J. A. *Glastech. Ber. Glass Sci. Technol.* **2000**, *73*, 89.
(24) Furukawa, T.; Fox, K. E.; White, W. B. *J. Chem. Phys.* **1981**, *75*, 3226. Kamitsos, E. I.; Kapoutsis, J. A.; Jain, H.; Hsieh, C. H. *J. Non-Cryst. Solids* **1994**, *171*, 31.
(25) Galeener, F. L. *J. Non-Cryst. Solids* **1982**, *49*, 53.
(26) Berger, A. J.; Wang, Y.; Sammeth, D. M.; Itzkan, I.; Kneipp, K.; Feld, M. S. *Appl. Spectrosc.* **1995**, *49*, 1164.
(27) Skuja, L.; Guttler, B. *Phys. Rev. Lett.* **1996**, *77*, 2093.
(28) Boizot, B.; Petite, G.; Ghaleb, D.; Reynard, B.; Calas, G. *J. Non-Cryst. Solids* **1999**, *243*, 268.
(29) An, H.; Fleming, S. *J. Opt. Soc. Am. B* **2006**, *23*, 2303.
(30) Prieto, X.; Linares, J. *Opt. Lett.* **1996**, *21*, 1363.
(31) Hetherrington, G.; Jack, K. H.; Ramsay, M. W. *Phys. Chem. Glasses* **1965**, *6*, 6.

JP1033905